Outsized contribution of the semi-arid ecosystems to interannual variability in North American ecosystems

B. Byrne[1], J. Liu[2], A. A. Bloom[2], K. W. Bowman[2], Z. Butterfield[3], J. Joiner[4], T. F. Keenan[5,6], G. Keppel-Aleks[3], N. C. Parazoo[2], and Y. Yin[7]

[1]NASA Postdoctoral Program Fellow, Jet Propulsion Laboratory, California Institute of Technology, CA, USA
[2]Jet Propulsion Laboratory, California Institute of Technology, CA, USA
[3]Department of Climate and Space Sciences and Engineering, University of Michigan, Ann Arbor, MI, USA
[4]Goddard Space Flight Center, Greenbelt, MD 20771, USA
[5]Earth and Environmental Sciences Area, Lawrence Berkeley National Laboratory, Berkeley, California, USA
[6]Department of Environmental Science, Policy and Management, University of California, Berkeley, Berkeley, California, USA
[7]Division of Geological and Planetary Sciences, California Institute of Technology, Pasadena, CA, USA

Key Points:

- GPP and NEE IAV in western North America is characterized by amplification in spring-summer, with enhance uptake in cooler-wetter conditions.
- GPP and NEE IAV in eastern North America is characterized by compensating anomalies between spring and summer, reducing annual net anomalies.
- Observation-based NEE and GPP IAV give greater sensitivity to temperature and moisture anomalies than MsTMIP mean in western North America.

Corresponding author: Brendan Byrne, `brendan.k.byrne@jpl.nasa.gov`

Abstract

Across North America, interannual variability (IAV) in gross primary production (GPP) and net ecosystem exchange (NEE), and their relationship with environmental drivers, are poorly understood. Here, we examine IAV in GPP and NEE and their relationship to environmental drivers using two state-of-the-science flux products: NEE constrained by surface and space-based atmospheric CO_2 measurements over 2010–2015 and satellite up-scaled GPP from FluxSat over 2001–2017. We show that the arid western half of North America provides a larger contribution to IAV in GPP (104% of east) and NEE (127% of east) than the eastern half, in spite of smaller magnitude of annual mean GPP and NEE. This occurs because anomalies in western North America are temporally coherent across the growing season leading to an amplification of GPP and NEE. In contrast, IAV in GPP and NEE over eastern North America are dominated by seasonal compensation effects, associated with opposite responses to temperature anomalies in spring and summer. Terrestrial biosphere models in the MsTMIP ensemble partially capture these differences between eastern and western North America, but generally underestimate the sensitivity of flux anomalies in western North America to variations in soil temperature and moisture by 0–31%. This suggests that ecosystems in western North America may be more sensitive to warming and increasing aridity than models predict, and that reductions in growing season productivity and carbon sequestration under climate change may be larger than predicted by models.

1 Introduction

Interannual variations (IAV) in carbon fluxes between terrestrial ecosystems and the atmosphere drive variations in the growth rate of atmospheric CO_2. Understanding the drivers of IAV in the carbon cycle is critical for understanding the response of ecosystems to climate change (Cox et al., 2013; Baldocchi et al., 2016; Niu et al., 2017). In this study, we examine the drivers of IAV in gross primary production (GPP) and net ecosystem exchange (NEE) over subtropical and temperate North America. In particular, we contrast IAV in the semi-arid western regions of North America with the wetter eastern areas of North America.

Semi-arid ecosystems are moisture limited ecosystems, and cover large portions of western North America. Globally, semi-arid ecosystems have been shown to play an outsized role in internnual variability (IAV) of the atmospheric CO_2 growth rate (Poulter et al., 2014; Ahlström et al., 2015; Huang et al., 2016; Z. Fu et al., 2017), relative to what would be expected given their productivity. The reason that these ecosystem experience such large IAV in CO_2 net uptake is thought to be linked to moisture availability (Huang et al., 2016). In these ecosystems, negative GPP anomalies are driven by warm-dry conditions and positive GPP anomalies are driven by cool-wet conditions (Ahlström et al., 2015). In turn, NEE anomalies in these ecosystems are strongly associated with variations in GPP (Ahlström et al., 2015). Still, the relative impact of these ecosystems on North American carbon fluxes is not well characterized.

Eastern North America is generally wetter than the west and is dominated by forest and cropland ecosystems. IAV in these ecosystems has been shown to have seasonally compensating effects, defined as temporally anti-correlated anomalies during a growing season. For example, a number of studies have found that enhanced GPP early in the growing season is associated with reduced GPP later in the growing season over midlatitude cropland and forest ecosystems (Buermann et al., 2013; Wolf et al., 2016; Buermann et al., 2018).There are several possible mechanisms for explaining seasonal compensation effects. Enhanced spring GPP is associated with warmer spring temperatures (Angert et al., 2005; Wolf et al., 2016). Warmer temperatures early in the growing season result in increased evapotranspiration leading to reduced soil moisture later in the growing season, which adversely impacts productivity (Parida & Buermann, 2014; Wolf et al., 2016). Direct phenological mechanisms may also contribute to seasonal compensation effects, as the timing of spring budburst and autumn senescence has been found to be correlated on the scale of individual organisms and the landscape (Y. S. Fu et al., 2014; Keenan & Richardson, 2015). The impact of seasonal compensation effects on annual GPP anomalies has been studied across northern forests and croplands using upscaled FLUXNET GPP (Buermann et al., 2013), NDVI (Buermann et al., 2018) and solar-induced fluorescence (SIF), while seasonal compensation in NEE has been examined for the 2012 North America drought (Wolf et al., 2016; J. Liu et al., 2018). However, the implications of seasonal compensation effects on variability in the carbon balance across multiple years over North America have not yet been examined.

In this study, we take advantage of two newly developed GPP and NEE products to examine IAV over North America. NEE fluxes are obtained from the inversion analyses of Byrne, Liu, et al. (2019). They estimated 14-day NEE globally over 2010–2015 in a flux inversion assimilating both surface-based and space-based CO_2 measurements. This combination of surface- and space-based measurements provides unprecedented observational coverage for a multi-year flux inversion and is expected to mitigate artifacts in the NEE fluxes that are introduced due to uneven observational coverage (J. Liu et al., 2014; Byrne et al., 2017). Using these NEE estimates in combination with 17 years (2001–2017) of satellite-based GPP calibrated on eddy covariance sites from FluxSat (Joiner et al., 2018), we examine the importance of seasonal compensation effects in GPP and NEE across North America. First, we examine the extent to which seasonal compensation effects impact growing season GPP and NEE anomalies across North America, and their dependence on temperature and moisture anomalies. Then, we examine the relative contribution of eastern and western North America to the mean seasonal cycle and IAV, and compare our data-driven estimates to modelled fluxes from the Multi-scale Synthesis and Terrestrial Model Intercomparison Project (MsTMIP).

2 Data

2.1 Carbon data

We employ two state-of-the-science observationally-constrained GPP and NEE products for examining IAV. The FluxSat GPP product (Sec. 2.1.1) (Joiner et al., 2018) is based on an up-scaling of global eddy covariance flux measurements, and has been found to produce more realistic IAV in GPP when compared to FLUXNET sites relative to other upscaled GPP products (Joiner et al., 2018). The flux inversion NEE product used here (Sec. 2.1.2) is unique in that it assimilates both surface- and space-based CO_2 measurements, providing increased observational constraints relative to other NEE flux inversion products. Atmospheric CO_2 fields simulated using this product have also been extensively evaluated against aircraft-based CO_2 measurements in the northern extratropics (Byrne, Liu, et al., 2019). In addition, we compare these observationally-constrained flux estimates to terrestrial biosphere model (TBM) estimates from the MsTMIP ensemble (Sec. 2.1.3).

2.1.1 FluxSat GPP

FluxSat version 1 (Joiner et al., 2018) estimates GPP based primarily on Nadir BRDF-Adjusted Reflectances (NBAR) from the MODerate-resolution Imaging Spectroradiometer (MODIS) MYD43D product (Schaaf et al., 2002) that uses data from MODIS instruments on National Aeronautics and Space Administration (NASA) Aqua and Terra satellites. The GPP estimates are calibrated with the FLUXNET 2015 GPP derived from eddy covariance flux measurements at Tier 1 sites (Baldocchi et al., 2001). As such, FluxSat can be considered as a global upscaling of the FLUXNET 2015 GPP data. The data set also employs SIF from the Global Ozone Monitoring Experiment 2 (GOME-2) on the EUMETSAT MetOp-A satellite to identify regions of high productivity crops. FluxSat was evaluated by comparison with independent flux measurements (i.e., not used in the training) and compared very well both in terms of IAV and site-to-site variability. Monthly mean FluxSat GPP data on a $0.5° \times 0.5°$ spatial grid were downloaded from https://avdc.gsfc.nasa.gov/pub/tmp/FluxSat_GPP and regridded to a $4° \times 5°$ spatial grid to for this analysis.

2.1.2 Flux inversion NEE

NEE fluxes are produced from a flux inversion analyses spanning 2010–2015. The flux inversions assimilate CO_2 measurements from the Greenhouse Gases Observing Satellite (GOSAT), Total Carbon Column Observing Network (TCCON), and the surface in situ and flask measurements network concurrently. Four dimensional variational (4-DVar) assimilation was implemented to estimate 14-day scaling factors for prior NEE and ocean fluxes at $4°\times5°$ spatial resolution using the Greenhouse gas framework - Flux model (GHGF-Flux). The optimized fluxes are taken to be the average of three flux inversions that employ different prior NEE fluxes and errors. NEE fluxes are aggregated to monthly mean values for this analysis. A detailed description of the experimental set up and evaluation of the fluxes can be found in Byrne, Liu, et al. (2019).

2.1.3 MsTMIP models

MsTMIP is a model inter-comparison experiment conducted by the North American Carbon Program (Huntzinger et al., 2013; Wei et al., 2014). The project is designed to provide a consistent and unified modeling framework in order to isolate, interpret, and address differences in process parameterizations among TBMs. In this analysis, we examine the modelled NEE (defined here as MsTMIP NEP$\times-1$) and GPP from the MsTMIP Version 1 SG3 simulation, in which the models are driven by CRU+NCEP reanalysis on a global $0.5° \times 0.5°$ spatial grid with time-varying land-use history and atmospheric CO_2, but with nitrogen deposition kept constant. We examine modeled fluxes over the period 1980–2010. These data were downloaded from the ORNL DAAC (Huntzinger et al., 2016). A list of models included in this study are shown in Fig. S8.

2.2 Environmental data

Anomalies in CO_2 fluxes are compared with anomalies in environmental variables that are expected to drive carbon cycle anomalies. In particular, we focus our analysis on the relationship between anomalies in CO_2 fluxes with anomalies in soil temperature and soil moisture.

2.2.1 Soil Temperature

Soil temperatures are from the MERRA-2 (Reichle et al., 2011, 2017; Gelaro et al., 2017) reanalysis. We average the soil temperature over levels 1–3 (TSOIL1,TSOIL2,and TSOIL3), which reaches a depth of 0.73 m. These data were downloaded from the Goddard Earth Sciences Data and Information Services Center at monthly temporal resolution and $4°\times5°$ spatial resolution (regridded from model horizontal resolution of $\sim$50 km).

2.2.2 Moisture stress variables

The ESA CCI combined surface soil moisture product (Y. Y. Liu et al., 2011, 2012) was downloaded from https://www.esa-soilmoisture-cci.org/. We use the combined active and passive soil moisture product. Daily soil moisture estimates are provided on a $0.25° \times 0.25°$ longitude–latitude spatial grid, but we regrid to monthly estimates on a $4° \times 5°$ spatial grid.

Additional datasets are used for supplemental analysis of the relationship between carbon fluxes and moisture stress. We obtain precipitation estimates from the Global Precipitation Climatology Project (GPCP) Monthly Analysis Product. We use GPCP Version 2.3 Combined Precipitation Dataset (Adler et al., 2003). We use RL06 monthly mass grids of terrestrial water storage (TWS) anomalies derived from the Gravity Recovery and Climate Experiment (GRACE) mission (Tapley et al., 2004; Flechtner et al., 2014; Landerer & Swenson, 2012).

3 Methods

3.1 Definition of anomalies

Anomalies are denoted with a "Δ" for all quantities (e.g., ΔNEE). To calculate anomalies, the mean seasonal cycle over a baseline period is removed. The baseline period employed is 2010–2015 for flux inversion NEE, 2003–2014 for GRACE TWS, and 2001–2017 for GPP, soil temperature, soil moisture, and precipitation. In addition, a linear trend is removed for all datasets except the NEE flux inversion (because the flux inversion timeseries is only six-years). Sensitivity tests found that results were not sensitive to the time period chosen for the baseline.

3.2 Quantifying IAV features

We focus our analysis on the seasonal compensation component and amplification component of IAV over the growing season. For NEE, we define the seasonal compensation component (NEE_{comp}) and seasonal amplification component (NEE_{amp}) as,

$$\Delta\text{NEE}_{\text{comp}} = \Delta\text{NEE}_{\text{Jul-Aug-Sep}} - \Delta\text{NEE}_{\text{Apr-May-Jun}}, \quad (1)$$

$$\Delta\text{NEE}_{\text{amp}} = \Delta\text{NEE}_{\text{Jul-Aug-Sep}} + \Delta\text{NEE}_{\text{Apr-May-Jun}}, \quad (2)$$

where $\Delta\text{NEE}_{\text{Apr-May-Jun}}$ and $\Delta\text{NEE}_{\text{Jul-Aug-Sep}}$ are the mean anomalies across April–June and July–September, respectively. A schematic of NEE anomalies leading to positive and negative amplification and compensation components are shown in Figure S1. The amplification component indicates a net increase or decrease in carbon uptake over the growing season. For example, if NEE anomalies are positive across the growing season (Fig. S1a), this will imply positive amplification and enhanced CO_2 emitted to the atmosphere ($\Delta\text{NEE}_{\text{amp}} > 0$). The compensation component indicates anti-correlated anomalies between the spring and summer. For example, if NEE anomalies are positive in the spring but negative in the summer (Fig. S1b), this will imply a negative compensation over the growing season ($\Delta\text{NEE}_{\text{comp}} < 0$). We define compensation and amplification for GPP in the same way.

We examine the relative magnitudes of these two components by taking the ratio of the mean absolute seasonal compensation component to the mean absolute amplification component. For NEE, this ratio is defined as:

$$\text{NEE}_{\text{RATIO}} = \frac{\sum_{\text{y}=2010}^{2015} |\Delta\text{NEE}_{\text{comp}}|}{\sum_{\text{y}=2010}^{2015} |\Delta\text{NEE}_{\text{amp}}|}. \quad (3)$$

The quantity $\text{NEE}_{\text{RATIO}}$ provides a measure of the relative magnitudes of the compensation and amplification components. If the magnitude of compensation is generally larger than amplification then the ratio will be larger than 1. If amplification dominates then the ratio will be less than 1.

Note that we split the growing season into the spring (April-May-June) and summer (July-August-September). The spring roughly covers the period from the spring equinox (March 20) to the summer solstice (June 20), while the summer roughly covers the period from the summer solstice to the fall equinox (Sep 22). We note that these definitions are lagged by one month from the meteorological seasons.

3.3 Singular value decomposition

We employ singular value decomposition (SVD) to examine the modes of variability in monthly ΔNEE and ΔGPP between years. SVD is a method to decompose a matrix into a set of singular vectors and singular values (Golub & Reinsch, 1971), where the singular vectors are a set of orthogonal basis vectors. In this analysis, we perform SVD on ΔGPP and ΔNEE arranged into month–by–year matrices. Thus, the singular vectors give the modes of monthly variability between years in ΔGPP and ΔNEE. The fraction of overall variance explained the leading singular vector "i" is then calculated using the expression $R^2 = s_i^2 / \sum_j s_j^2$, where s_j are the singular values.

4 Results

4.1 Amplification dominates in the west and compensation dominates in the East

We examine the relative magnitudes of seasonal compensation and amplification in ΔGPP and ΔNEE. Figure 1 shows $\mathrm{NEE_{RATIO}}$ for 2010–2015 and $\mathrm{GPP_{RATIO}}$ for 2001–2017 over subtropical and temperate North America ($\mathrm{GPP_{RATIO}}$ for 2010–2015 is shown in Fig. S2). Spatially, seasonal compensation is most dominant in eastern North America (largest ratios), particularly around the Midwest. In contrast, the amplification component of IAV is most dominant in western North America, particularly in the southwest. Figure 1c and 1d show $\mathrm{NEE_{RATIO}}$ and $\mathrm{GPP_{RATIO}}$ as a function of the mean Apr-Sep soil moisture and soil temperature for each $4^\circ \times 5^\circ$ grid cell. Larger ratios are found to cluster in the wetter areas while smaller ratios are generally found in the drier areas, consistent with the climatological difference between the west and east of North America. In support of these results, similar spatial structure for $\mathrm{NEE_{RATIO}}$ is obtained using the independent NOAA's CarbonTracker flux inversion, version CT2017 with updates documented at http://carbontracker.noaa.gov (Peters et al., 2007) (Fig. S3). In addition, the $\mathrm{GPP_{RATIO}}$ spatial structure is supported by GOME–2 version 28 (V28) 740 nm terrestrial SIF data (Joiner et al., 2013, 2016), while agreement with FLUXCOM GPP (Tramontana et al., 2016) is mixed (Fig. S4).

To further examine differences in IAV between eastern and western North America, we aggregate gridcells into western and eastern regions (Fig. 2a). We then perform SVD on matrices of monthly ΔNEE and ΔGPP (with months as the rows and years as columns) over these two regions. This analysis allows us to compute basis vectors that explain modes of variability in monthly ΔNEE and ΔGPP between years. The first and second basis vectors, which explain the majority of variability in ΔNEE and ΔGPP are shown in Fig. 2. These basis vectors show that the western region is dominated by amplification in GPP and NEE, with the first singular value explaining 66% and 76% of the variance, respectively (Fig. 2). Conversely, the eastern region is dominated by seasonal compensation in GPP and NEE, with the first singular value explaining 59% and 47% of the variance, respectively (Fig. 2). Thus, these aggregated regions are generally reflective of the IAV seen at the grid cell level.

4.2 Relationship between flux anomalies and environmental drivers

To a large extent, IAV in the carbon balance of ecosystems is expected to be driven by IAV in temperature and moisture (Berry & Bjorkman, 1980; Smith et al., 2011; Byrne, Jones, et al., 2019), thus we examine the relationship between CO_2 flux anomalies and anomalies in soil temperature (ΔT) and soil moisture (ΔM). Figure 3 shows the correlation between ΔGPP and anomalies in climate variables over 2001–2017. Note that we correlated Jul–Sep flux anomalies with Apr–Sep climate anomalies to incorporate lagged effects of spring climate anomalies on summer carbon cycle anomalies. We find spatial differences in the correlation coefficient between western and eastern North America. In

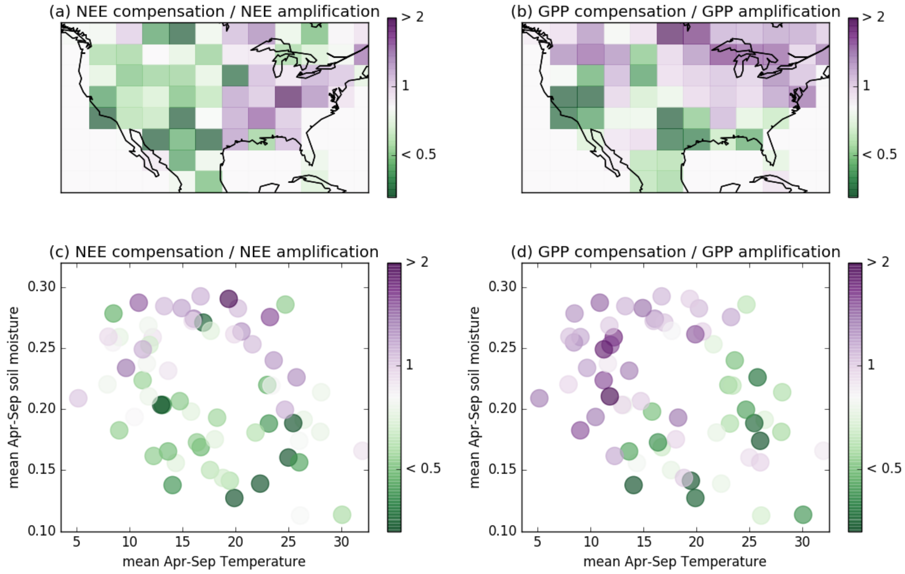

Figure 1. Relative magnitudes of seasonal compensation and amplification. (a) NEE_{RATIO} over 2010–2015 and (b) GPP_{RATIO} over 2001–2017 at $4^{\circ} \times 5^{\circ}$. (c) NEE_{RATIO} and (d) GPP_{RATIO} plotted as a function of Apr-Sep mean soil temperature and soil moisture.

the west, increased GPP (positive ΔGPP) is found to be correlated with cooler (negative ΔT) and wetter (positive ΔM) conditions during both Apr–Jun and Jul–Sep. The temporally coherent relationship between flux anomalies and environmental anomalies in western North America suggests that cooler-wetter years will lead to an amplification of carbon uptake. In the east, increased GPP is correlated with warmer conditions during Apr–Jun, but cooler and wetter conditions during Jul–Sep. These seasonal variations in the relationship between flux anomalies and environmental variables suggest that seasonal compensation will occur when climate anomalies persist throughout the year. For example, warm years would result in increased uptake during the spring but decreased uptake during the summer. Similar results are found for NEE (Fig. S5) over 2010-2015, although correlations are generally less statistically significant. This is likely partially explained by the shorter time period examined and the inability of the flux inversion to isolate NEE anomalies to $4^{\circ} \times 5^{\circ}$ spatial grid cells.

We now examine the seasonal cycles of GPP and NEE over the western and eastern regions of North America. Figure 4 shows the seasonal cycles of GPP (2001–2017) and NEE (2010–2015) over the western and eastern regions of North America with different years coloured by the corresponding Apr-Sep ΔT or ΔM. An additional plot showing the seasonal compensation and amplification components as a function of ΔT or ΔM is shown in the supplementary materials (Fig. S6). For western North America, variations in the seasonal cycle of GPP and NEE are dominated by an amplification component over Apr-Sep. Increased GPP and net uptake are associated with cooler and wetter conditions. ΔT and ΔM are strongly correlated with each other ($R = -0.77$ for 2001–2017), obscuring which variable has the largest impact on IAV. However, the magnitude of the correlation is slightly larger for ΔM as compared with ΔT for ΔNEE_{amp} (0.91 vs 0.71) and ΔGPP_{amp} (0.66 vs 0.63) (Table S1). IAV is generally weaker in eastern North America (relative to the mean seasonal cycle). Temporal shifts in the seasonal cycle of GPP (ΔGPP_{comp}) and NEE (ΔNEE_{comp}) provide the largest component of IAV. Shifts of GPP and NEE to earlier in the year are associated with positive Apr-Sep ΔT (Fig. 4b (i) and (iii)), suggesting that a warm spring drives the shift and persistent warming dur-

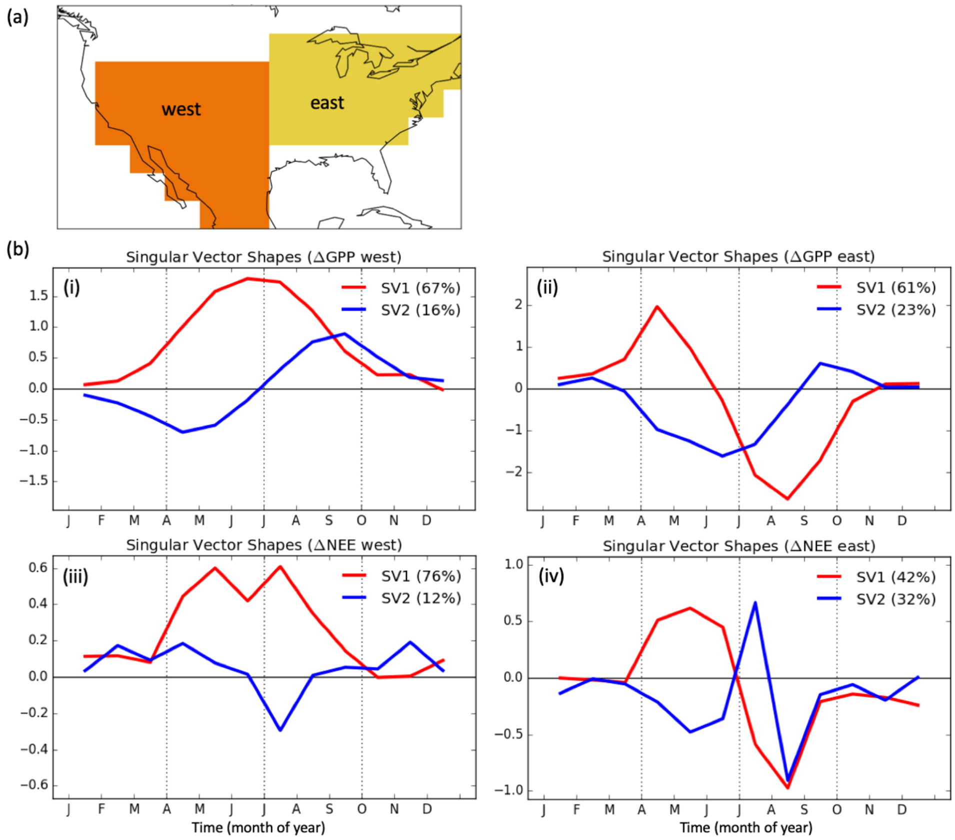

Figure 2. (a) The spatial extent of western (orange) and eastern (yellow) regions of North America. (b) First and second singular vectors resulting from the decomposition of the IAV in GPP over 2001–2017 for the (i) western and (ii) eastern regions of North America, and of the IAV in NEE over 2010–2015 for the (iii) western and (iv) eastern regions of North America.

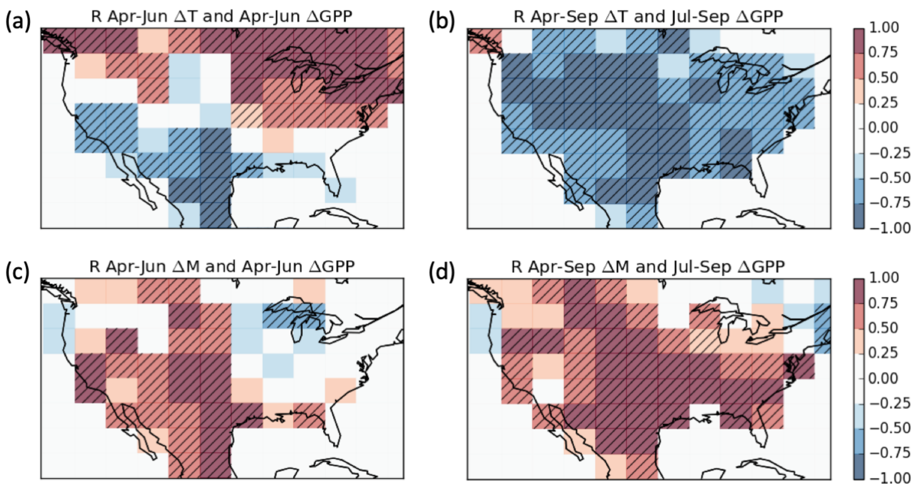

Figure 3. Relationship between ΔGPP and variations in climate. Coefficient of correlation (R) over 2001-2017 for $4^\circ \times 5^\circ$ grid cells between (a) Apr–Jun ΔT and Apr–Jun ΔGPP, (b) Apr-Sep ΔT and Jul–Sep ΔGPP, (c) Apr–Jun ΔM and Apr–Jun ΔGPP and (d) Apr-Sep ΔM and Jul–Sep ΔGPP. Hatching shows grid cells for which $P < 0.05$.

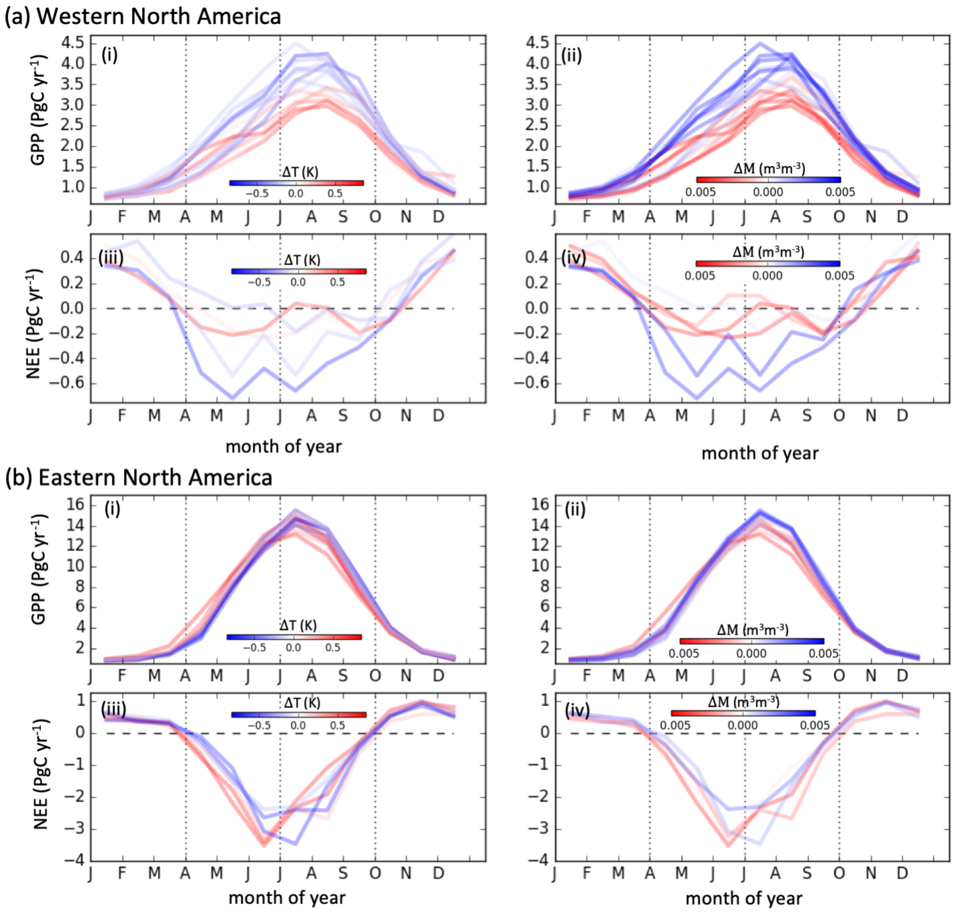

Figure 4. Seasonal cycles of GPP (2001–2017) and NEE (2010-2015) over eastern and western North America. (a) Seasonal cycles of (i-ii) GPP and (iii-iv) NEE over western North America. (b) Seasonal cycles of (i-ii) GPP and (iii-iv) NEE over eastern North America. Colors indicate the Apr-Sep ΔT ((i) and (iii)) or Apr-Sep ΔM ((ii) and (iv)).

ing summer reduces the productivity and net uptake. Variations in Apr-Sep ΔM are more closely tied to an amplification component of ΔGPP (R=0.72) and ΔNEE (R=0.78) (Table S1). This implies that increased soil moisture is associated with increased GPP but reduced net uptake, suggesting that respiration fluxes increase more than GPP with increased soil moisture. This result is consistent with Z. Liu et al. (2018), but contradicted (for droughts) by Schwalm et al. (2010). Thus, more research is needed on this topic.

4.3 Impact of amplification and compensation for net CO_2 fluxes

The presence of temporally coherent spring–summer flux anomalies in western North America acts to increase the annual net flux anomalies. In contrast, anti-correlated spring–summer flux anomalies in eastern North America acts to reduce the net annual flux anomalies. Here we examine the relative contribution of eastern and western North America to the mean seasonal cycle and anomalies of GPP and NEE (Figure 5). We find that monthly NEE and GPP fluxes are larger in eastern North America than in western North America (7.6$\times$ for GPP, 3.5$\times$ for NEE), reflecting a more productive carbon cycle. However, due to seasonal compensating anomalies, annual anomalies in GPP and NEE are larger in the west than the east (1.04$\times$ for GPP and 1.27$\times$ for NEE). Thus, growing season

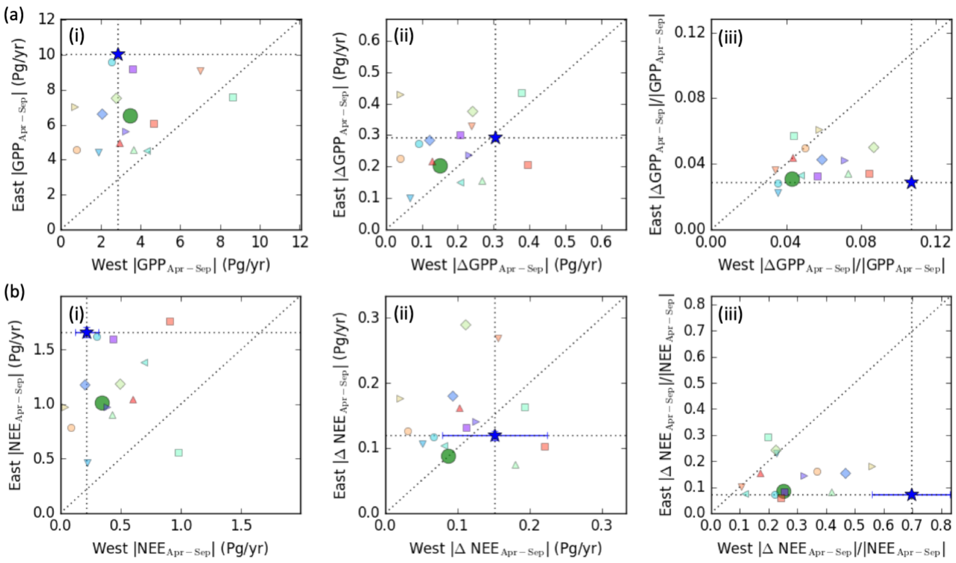

Figure 5. Scatter plots of (a) GPP and (b) NEE fluxes in eastern and western North America. The panels show (i) the magnitude of Apr-Sep mean fluxes, (ii) the magnitude of Apr-Sep mean anomalies, and (iii) the ratio of the anomalies to mean fluxes. The blue star shows the observationally-based estimates from FluxSat GPP and the flux inversion NEE. The error bars on the observationally-constrained NEE estimate show the range in these values between the three flux inversions from (Byrne, Liu, et al., 2019), note error bars are very small for the east. The large green circle shows the GPP and NEE estimate from the MsTMIP model mean. Small circles show the GPP and NEE estimates from individual MsTMIP models.

IAV in NEE and GPP is larger in the western North America, despite a more productive carbon cycle in eastern North America. The impacts of these differences in IAV between these two regions are evident in the timeseries of ΔGPP and ΔNEE anomalies two regions (Fig. S7). Monthly anomalies in western North America are coherent for individual years leading to increased annual anomalies, while anomalies in the east show seasonal compensation, reducing annual net anomalies.

We now investigate the ability of the MsTMIP models to recover observationally-constrained west-east differences in GPP and NEE over 1980–2010. Modeled fluxes are plotted with the observationally-constrained estimates in Fig 5. The MsTMIP models systematically underestimate the magnitude of Apr-Sep GPP and NEE in eastern North America relative to FluxSat GPP and inversion NEE, but closely agree with the observationally-constrained fluxes in western North America. The mean magnitudes of Apr-Sep ΔGPP and ΔNEE are variable between MsTMIP models, but are generally smaller than the observationally-based estimates. The model mean gives similar magnitudes of ΔGPP and ΔNEE in eastern and western North America, suggesting that the models at-least partially capture increased IAV in western North America. The ratio of the magnitudes of Apr-Sep IAV to the Apr-Sep mean are shown in Fig. 5c. The models systematically underestimate this ratio for GPP and NEE in western North America. The MsTMIP models predict that mean magnitude of Apr-Sep ΔGPP is 4% (range of 3–9%) of the Apr-Sep GPP, while FluxSat GPP suggests 11%. Similarly, MsTMIP models predict that mean magnitude of Apr-Sep ΔNEE is 25% (range of 11–56%) of the Apr-Sep NEE, while inversion NEE suggests 70%. The MsTMIP model mean also tends to give weaker sensitivity to soil moisture and temperature anomalies (Table 1). FluxSat ΔGPP is found to be about 30% more sensitive to variations in soil temperature and moisture than the

Table 1. Observationally-based and model based sensitivities. Slope and R^2 values for linear regressions of Apr-Sep ΔGPP and ΔNEE against Apr-Sep ΔT and ΔM for FluxSat GPP (2001–2017), inversion NEE (2010–2016), and MsTMIP model mean GPP and NEE (2001–2010). MsTMIP fluxes are examined over 2001–2010 to isolate comparisons to the period when observational datasets are best constrained by observations. Bold numbers indicate P<0.05.

	West				East			
	Temperature		Soil Moisture		Temperature		Soil Moisture	
	slope (PgC K^{-1})	R^2	slope (PgC $(m^3m^{-3})^{-1}$)	R^2	slope PgC K^{-1}	R^2	slope (PgC $(m^3m^{-3})^{-1}$)	R^2
FluxSat ΔGPP	-0.29	0.44	**32.6**	**0.89**	-0.04	0.03	52.2	0.09
Model ΔGPP	**-0.20**	**0.55**	**23.4**	**0.91**	-0.02	0.02	**110.6**	**0.45**
Inversion ΔNEE	0.13	0.47	-10.3	0.49	-0.04	0.19	28.6	0.21
Model ΔNEE	**0.11**	**0.53**	**-10.3**	**0.71**	**0.06**	**0.60**	**-53.5**	**0.42**

MsTMIP model mean, while inversion ΔNEE variations are 15% larger for soil temperature than the MsTMIP model mean but identical for soil moisture. In eastern North America, the MsTMIP models suggest greater sensitivity to environmental variables than the observationally-constrained fluxes (Table 1), as previously suggested by Shiga et al. (2018).

5 Discussion

5.1 Mechanisms driving IAV

5.1.1 Western North America

We find that IAV in western North America is dominated by an amplification component, wherein increased GPP and net uptake are associated with cooler-wetter conditions. This result is consistent with a number of previous studies investigating southwest North America (Zhang et al., 2013; Parazoo et al., 2015; Papagiannopoulou et al., 2017; Shiga et al., 2018; Hu et al., 2019) and in semi-arid regions more broadly (Poulter et al., 2014; Ahlström et al., 2015; Huang et al., 2016; Z. Fu et al., 2017). Variations in GPP and NEE over this region are likely primarily due to variations in water availability, rather than temperature variability (Papagiannopoulou et al., 2017). Parazoo et al. (2015) have shown that variability in productivity over the Southern US – Northern Mexico region is linked to El Nino Southern Oscillation (ENSO) and the North Atlantic Oscillation (NAO), and suggest that year-to-year variability of carbon net uptake is associated with precipitation anomalies in this region. We find ΔP is strongly correlated with ΔGPP_{amp} (R=0.78) and moderately correlated with ΔNEE_{amp} (R=-0.47) in western North America (Table S1). This suggests that IAV in western North America is primarily driven by large scale climate variability. Supporting this result, Hu et al. (2019) found that North American net uptake is correlated with ENSO phase, which they primarily attributed to variations in water availability.

5.1.2 Eastern North America

We find that GPP and NEE IAV in eastern North America are dominated by a seasonal compensation component, where an increase in Apr–Jun is followed by a compensating decrease in Jul–Sep. This is most closely linked to a shift of the seasonal cycle to earlier in the year with increased temperature. This phenomena has previously been reported for studies of phenology (Y. S. Fu et al., 2014; Keenan & Richardson, 2015), GPP

(Buermann et al., 2013, 2018; Parida & Buermann, 2014; Papagiannopoulou et al., 2017) and NEE (Wolf et al., 2016; J. Liu et al., 2018; Shiga et al., 2018; Rödenbeck et al., 2018; Hu et al., 2019). Most studies attribute this phenomena to land-atmosphere interactions, wherein a warm spring results in drying and drought during the summer (Parida & Buermann, 2014; Wolf et al., 2016). This explanation is generally consistent with our results for GPP but not for NEE. We find that Apr–Jun ΔGPP and ΔNEE are correlated with Apr–Jun ΔT (R=0.86 for GPP, R=-0.95 for NEE) but only Jul–Sep ΔGPP is correlated with Jul–Sep ΔM (R=0.72 for GPP, R=0.16 for NEE). A further difficulty with this mechanism explaining seasonal compensation effects is that Apr–Jun ΔT and Jul–Sep ΔM are only weakly correlated over eastern North America (R=-0.28). This is true for grid cells with cropland fractions greater than 65% (R=-0.19) and less than 35% (R=-0.28) (see Fig. S9). To some extent, the lack of correlation could be due to errors in the ESA CCI soil moisture product, as somewhat stronger correlations are found between Apr–Jun ΔT and Jul–Sep GRACE ΔTWS (R=-0.44 for 2003–2014, Table S1). Still, these results suggests that other factors play a role in seasonal compensation effects. Direct physiological mechanisms linking budburst and senescence, such as leaf structure constraints on longevity (Reich et al., 1992) or programmed cell death (Lam, 2004), may have a significant impact on the length of the growing season (Keenan & Richardson, 2015). However, more research is needed to understand the drivers of seasonal compensation effects.

5.2 Implications for North American carbon sink

The sensitivity of carbon cycle IAV to environmental drivers may provide information on the sensitivity of the carbon cycle to climate change (Cox et al., 2013). Here, we discuss the implications of the relationships between carbon cycle IAV and environmental drivers for the future carbon balance of North America under anthropogenic climate change.

Changes in temperature and the water cycle of North America have been observed and are projected into the future. The annual average temperature of the contiguous US has risen by 0.7–1.0 °C since the start of the 20th century, and is projected to increase by 1.4 °C (RCP4.5) to 1.6 °C (RCP8.5) for 2021–2050 relative to 1976–2005, based on Coupled Model Intercomparison Project 5 (CMIP5) simulations (Vose et al., 2017). Warming is driving a more rapid water cycle (Huntington et al., 2018). This is projected to cause decreases in soil moisture because increases in evapotranspiration (due to temperature increases) are expected to be larger than precipitation increases (Cook et al., 2015). Predicted warming and drying in western North America (Seager et al., 2007) could have profound effects on the carbon cycle (Schwalm et al., 2012), with increasing temperatures and aridity driving reductions in growing season productivity and carbon uptake. TBMs suggest that carbon loss due to climate change will be partially mitigated by increasing CO_2 (Huntzinger et al., 2018); however, given that the models are found to be less sensitive to climate variability than the observationally-constrained estimate, carbon loss may be underestimated. In eastern North America, the results of this study suggest that temperature increases will result in a shift of the growing season to earlier in the year, with increased uptake during the spring but decreased uptake during the summer. However, the observationally-constrained flux estimates do not show sensitivity of Apr-Sep net GPP and NEE to environmental anomalies, suggesting that eastern North American ecosystems may be more resilient to climate change than simulated by the models.

6 Conclusions

Observationally-constrained FluxSat GPP and CO_2 flux inversion NEE show that there are substantial differences in IAV between the arid west and wetter east of North

America. In western North America, spring and summer anomalies are found to be correlated, such that IAV is characterized by an amplification of the mean GPP and NEE during the growing season. These western ecosystems are generally water limited, such that increased GPP and net uptake are associated with cooler-wetter conditions. In eastern North America, spring and summer anomalies are anti-correlated, leading to compensating anomalies over the growing season. Anomalies in GPP and NEE are closely associated to temperature, with a shift in the seasonal cycle to earlier in the year during warm years, resulting in increased GPP and net uptake in Apr–Jun but decreased GPP and net uptake in Jun-Sep.

Due to the dominance of amplification in the west and seasonal compensation in the east, western North America contributes more to IAV than the eastern North America in GPP (104% of east) and NEE (127% of east) during the growing season (April-September), despite the fact that the mean growing season fluxes are larger in the east (7.6$\times$ for GPP, 3.5$\times$ for NEE). Simulated GPP and NEE from the MsTMIP ensemble partially recover the larger IAV in the west relative to the east, but underestimate the magnitude of this effect. In particular, the MsTMIP model mean tends to underestimate the sensitivity of western ecosystems to variation in soil temperature and soil moisture (by 0–31%). These results suggest that ecosystems in western North America could be sensitive to increases in temperature and aridity expected under climate change, and that reductions in growing season productivity and net uptake could be larger than simulated by TBMs.

Acknowledgments

BB was supported by an appointment to the NASA Postdoctoral Program at the Jet Propulsion Laboratory, administered by Universities Space Research Association under contract with NASA. JL was supported by the NASA OCO2/3 science team program NNH17ZDA001N-OCO2. JJ was supported by NASA through the Earth Science U.S. Participating Investigator and Making Earth Science Data Records for Use in Research Environments (MEaSUREs) programs. TFK was supported by the NASA Terrestrial Ecology Program IDS Award NNH17AE86I. Resources supporting this work were provided by the NASA High-End Computing (HEC) Program through the NASA Advanced Supercomputing (NAS) Division at Ames Research Center. Funding for the Multi-scale synthesis and Terrestrial Model Intercomparison Project (MsTMIP; https://nacp.ornl.gov/MsTMIP.shtml) activity was provided through NASA ROSES Grant #NNX10AG01A. Data management support for preparing, documenting, and distributing model driver and output data was performed by the Modeling and Synthesis Thematic Data Center at Oak Ridge National Laboratory (ORNL; http://nacp.ornl.gov), with funding thorugh NASA ROSES Grant #NNH10AN681. Finalized MsTMIP data products are archived at the ORNL DAAC (http://daac.ornl.gov). The research was carried out at the Jet Propulsion Laboratory, California Institute of Technology, under a contract with the National Aeronautics and Space Administration (80NM0018D004).

References

Adler, R. F., Huffman, G. J., Chang, A., Ferraro, R., Xie, P.-P., Janowiak, J., ... others (2003). The version-2 Global Precipitation Climatology Project (GPCP) monthly precipitation analysis (1979–present). *J. Hydrometeor.*, *4*(6), 1147–1167.

Ahlström, A., Raupach, M. R., Schurgers, G., Smith, B., Arneth, A., Jung, M., ... others (2015). The dominant role of semi-arid ecosystems in the trend and variability of the land CO_2 sink. *Science*, *348*(6237), 895–899.

Angert, A., Biraud, S., Bonfils, C., Henning, C., Buermann, W., Pinzon, J., ... Fung, I. (2005). Drier summers cancel out the co2 uptake enhancement induced by warmer springs. *Proceedings of the National Academy of Sciences*,

102(31), 10823–10827.
Baldocchi, D., Falge, E., Gu, L., Olson, R., Hollinger, D., Running, S., ... others (2001). FLUXNET: A new tool to study the temporal and spatial variability of ecosystem–scale carbon dioxide, water vapor, and energy flux densities. *B. Am. Meteorol. Soc.*, *82*(11), 2415–2434.
Baldocchi, D., Ryu, Y., & Keenan, T. (2016). Terrestrial carbon cycle variability. *F1000Research*, *5*.
Berry, J., & Bjorkman, O. (1980). Photosynthetic response and adaptation to temperature in higher plants. *Ann. Rev. Plant Physio.*, *31*(1), 491–543.
Buermann, W., Bikash, P. R., Jung, M., Burn, D. H., & Reichstein, M. (2013). Earlier springs decrease peak summer productivity in north american boreal forests. *Environmental Research Letters*, *8*(2), 024027.
Buermann, W., Forkel, M., O'Sullivan, M., Sitch, S., Friedlingstein, P., Haverd, V., ... others (2018). Widespread seasonal compensation effects of spring warming on northern plant productivity. *Nature*, *562*(7725), 110.
Byrne, B., Jones, D. B. A., Strong, K., Polavarapu, S. M., Harper, A. B., Baker, D. F., & Maksyutov, S. (2019). On what scales can gosat flux inversions constrain anomalies in terrestrial ecosystems? *Atmos. Chem. Phys. Discuss.*, *2019*, 1–42. Retrieved from `https://www.atmos-chem-phys-discuss.net/acp-2018-909/` doi: 10.5194/acp-2018-909
Byrne, B., Jones, D. B. A., Strong, K., Zeng, Z.-C., Deng, F., & Liu, J. (2017). Sensitivity of CO_2 surface flux constraints to observational coverage. *J. Geophys. Res.-Atmos*, *112*(12), 6672–6694. doi: 10.1002/2016JD026164
Byrne, B., Liu, J., Lee, M., Baker, I. T., Bowman, K. W., Deutscher, N. M., ... Wunch, D. (2019). Improved constraints on northern extratropical co2 fluxes obtained by combining surface-based and space-based atmospheric co2 measurements. *Earth and Space Science Open Archive*. doi: 10.1002/essoar.10501108.2
Cook, B. I., Ault, T. R., & Smerdon, J. E. (2015). Unprecedented 21st century drought risk in the american southwest and central plains. *Science Advances*, *1*(1), e1400082.
Cox, P. M., Pearson, D., Booth, B. B., Friedlingstein, P., Huntingford, C., Jones, C. D., & Luke, C. M. (2013). Sensitivity of tropical carbon to climate change constrained by carbon dioxide variability. *Nature*, *494*(7437), 341–344.
Flechtner, F., Morton, P., Watkins, M., & Webb, F. (2014). Status of the grace follow-on mission. In *Gravity, geoid and height systems* (pp. 117–121). Springer.
Fu, Y. S., Campioli, M., Vitasse, Y., De Boeck, H. J., Van den Berge, J., AbdElgawad, H., ... Janssens, I. A. (2014). Variation in leaf flushing date influences autumnal senescence and next year's flushing date in two temperate tree species. *Proceedings of the National Academy of Sciences*, *111*(20), 7355–7360.
Fu, Z., Dong, J., Zhou, Y., Stoy, P. C., & Niu, S. (2017). Long term trend and interannual variability of land carbon uptake - the attribution and processes. *Environmental Research Letters*, *12*(1), 014018.
Gelaro, R., McCarty, W., Suárez, M. J., Todling, R., Molod, A., Takacs, L., ... others (2017). The modern-era retrospective analysis for research and applications, version 2 (MERRA-2). *J. Climate*, *30*(14), 5419–5454.
Golub, G. H., & Reinsch, C. (1971). Singular value decomposition and least squares solutions. In *Linear algebra* (pp. 134–151). Springer.
Hu, L., Andrews, A. E., Thoning, K. W., Sweeney, C., Miller, J. B., Michalak, A. M., ... others (2019). Enhanced north american carbon uptake associated with el niño. *Science advances*, *5*(6), eaaw0076.
Huang, L., He, B., Chen, A., Wang, H., Liu, J., Lű, A., & Chen, Z. (2016). Drought dominates the interannual variability in global terrestrial net primary production by controlling semi-arid ecosystems. *Scientific reports*, *6*, 24639.

Huntington, T. G., Weiskel, P. K., Wolock, D. M., & McCabe, G. J. (2018). A new indicator framework for quantifying the intensity of the terrestrial water cycle. *Journal of hydrology*, *559*, 361–372.

Huntzinger, D. N., Chatterjee, A., et al. (2018). Chapter 19: Future of the north american carbon cycle. *Second State of the Carbon Cycle Report (SOCCR2): A Sustained Assessment Report. US Global Change Research Program, Washington, DC, USA*, 760–809.

Huntzinger, D. N., Schwalm, C., Michalak, A. M., Schaefer, K., King, A. W., Wei, Y., ... Zhu, Q. (2013). The north american carbon program multi-scale synthesis and terrestrial model intercomparison project – part 1: Overview and experimental design. *Geoscientific Model Development*, *6*(6), 2121–2133. Retrieved from https://www.geosci-model-dev.net/6/2121/2013/ doi: 10.5194/gmd-6-2121-2013

Huntzinger, D. N., Schwalm, C., Wei, Y., Cook, R., Michalak, A., Schaefer, K., ... others (2016). *Nacp mstmip: Global 0.5-deg terrestrial biosphere model outputs (version 1) in standard format, data set.* ORNL DAAC, Oak Ridge, Tennessee, USA. doi: 10.3334/ORNLDAAC/1225

Joiner, J., Guanter, L., Lindstrot, R., Voigt, M., Vasilkov, A., Middleton, E., ... Frankenberg, C. (2013). Global monitoring of terrestrial chlorophyll fluorescence from moderate spectral resolution near-infrared satellite measurements: Methodology, simulations, and application to GOME-2. *Atmos. Meas. Tech.*, *6*(2), 2803–2823. doi: 10.5194/amt-6-2803-2013

Joiner, J., Yoshida, Y., Guanter, L., & Middleton, E. M. (2016). New methods for the retrieval of chlorophyll red fluorescence from hyperspectral satellite instruments: simulations and application to GOME-2 and SCIAMACHY. *Atmos. Meas. Tech.*, *9*(8), 3939–3967. Retrieved from https://www.atmos-meas-tech.net/9/3939/2016/ doi: 10.5194/amt-9-3939-2016

Joiner, J., Yoshida, Y., Zhang, Y., Duveiller, G., Jung, M., Lyapustin, A., ... Tucker, C. (2018). Estimation of terrestrial global gross primary production (GPP) with satellite data-driven models and eddy covariance flux data. *Remote Sensing*, *10*(9), 1346.

Keenan, T. F., & Richardson, A. D. (2015). The timing of autumn senescence is affected by the timing of spring phenology: implications for predictive models. *Global change biology*, *21*(7), 2634–2641.

Lam, E. (2004). Controlled cell death, plant survival and development. *Nature Reviews Molecular Cell Biology*, *5*(4), 305.

Landerer, F. W., & Swenson, S. (2012). Accuracy of scaled grace terrestrial water storage estimates. *Water resources research*, *48*(4).

Liu, J., Bowman, K., Parazoo, N. C., Bloom, A. A., Wunch, D., Jiang, Z., ... Schimel, D. (2018). Detecting drought impact on terrestrial biosphere carbon fluxes over contiguous us with satellite observations. *Environmental Research Letters*, *13*(9), 095003.

Liu, J., Bowman, K. W., Lee, M., Henze, D. K., Bousserez, N., Brix, H., ... others (2014). Carbon monitoring system flux estimation and attribution: impact of ACOS-GOSAT XCO_2 sampling on the inference of terrestrial biospheric sources and sinks. *Tellus B*, *66*(1), 22486. doi: 10.3402/tellusb.v66.22486

Liu, Y. Y., Dorigo, W. A., Parinussa, R., de Jeu, R. A., Wagner, W., McCabe, M. F., ... Van Dijk, A. (2012). Trend-preserving blending of passive and active microwave soil moisture retrievals. *Remote Sens. Environ.*, *123*, 280–297.

Liu, Y. Y., Parinussa, R., Dorigo, W. A., De Jeu, R. A., Wagner, W., Van Dijk, A., ... Evans, J. (2011). Developing an improved soil moisture dataset by blending passive and active microwave satellite-based retrievals. *Hydrol. Earth Syst. Sc.*, *15*(2), 425–436.

Liu, Z., Ballantyne, A. P., Poulter, B., Anderegg, W. R., Li, W., Bastos, A., & Ciais, P. (2018). Precipitation thresholds regulate net carbon exchange at the continental scale. *Nature communications*, *9*(1), 3596.

Niu, S., Fu, Z., Luo, Y., Stoy, P. C., Keenan, T. F., Poulter, B., ... others (2017). Interannual variability of ecosystem carbon exchange: From observation to prediction. *Global ecology and biogeography*, *26*(11), 1225–1237.

Papagiannopoulou, C., Miralles, D., Dorigo, W. A., Verhoest, N., Depoorter, M., & Waegeman, W. (2017). Vegetation anomalies caused by antecedent precipitation in most of the world. *Environmental Research Letters*, *12*(7), 074016.

Parazoo, N. C., Barnes, E., Worden, J., Harper, A. B., Bowman, K. B., Frankenberg, C., ... Keenan, T. F. (2015). Influence of enso and the nao on terrestrial carbon uptake in the texas-northern mexico region. *Global Biogeochemical Cycles*, *29*(8), 1247–1265.

Parida, B. R., & Buermann, W. (2014). Increasing summer drying in north american ecosystems in response to longer nonfrozen periods. *Geophysical Research Letters*, *41*(15), 5476–5483.

Peters, W., Jacobson, A. R., Sweeney, C., Andrews, A. E., Conway, T. J., Masarie, K., ... others (2007). An atmospheric perspective on North American carbon dioxide exchange: CarbonTracker. *Proc. Natl. Acad. Sci.*, *104*(48), 18925–18930. doi: 10.1073/pnas.0708986104

Poulter, B., Frank, D., Ciais, P., Myneni, R. B., Andela, N., Bi, J., ... others (2014). Contribution of semi-arid ecosystems to interannual variability of the global carbon cycle. *Nature*, *509*(7502), 600.

Reich, P. B., Walters, M., & Ellsworth, D. (1992). Leaf life-span in relation to leaf, plant, and stand characteristics among diverse ecosystems. *Ecological monographs*, *62*(3), 365–392.

Reichle, R. H., Draper, C. S., Liu, Q., Girotto, M., Mahanama, S. P., Koster, R. D., & De Lannoy, G. J. (2017). Assessment of MERRA-2 land surface hydrology estimates. *J. Climate*, *30*(8), 2937–2960.

Reichle, R. H., Koster, R. D., De Lannoy, G. J., Forman, B. A., Liu, Q., Mahanama, S. P., & Touré, A. (2011). Assessment and enhancement of MERRA land surface hydrology estimates. *J. Climate*, *24*(24), 6322–6338.

Rödenbeck, C., Zaehle, S., Keeling, R., & Heimann, M. (2018). How does the terrestrial carbon exchange respond to inter-annual climatic variations? A quantification based on atmospheric CO_2 data. *Biogeosciences*, *15*(8), 2481–2498. Retrieved from `https://www.biogeosciences.net/15/2481/2018/` doi: 10.5194/bg-15-2481-2018

Schaaf, C. B., Gao, F., Strahler, A. H., Lucht, W., Li, X., Tsang, T., ... others (2002). First operational brdf, albedo nadir reflectance products from modis. *Remote sensing of Environment*, *83*(1-2), 135–148.

Schwalm, C. R., Williams, C. A., Schaefer, K., Arneth, A., Bonal, D., Buchmann, N., ... others (2010). Assimilation exceeds respiration sensitivity to drought: A fluxnet synthesis. *Global Change Biology*, *16*(2), 657–670.

Schwalm, C. R., Williams, C. A., Schaefer, K., Baldocchi, D., Black, T. A., Goldstein, A. H., ... others (2012). Reduction in carbon uptake during turn of the century drought in western north america. *Nature Geoscience*, *5*(8), 551.

Seager, R., Ting, M., Held, I., Kushnir, Y., Lu, J., Vecchi, G., ... others (2007). Model projections of an imminent transition to a more arid climate in southwestern north america. *Science*, *316*(5828), 1181–1184.

Shiga, Y. P., Michalak, A. M., Fang, Y., Schaefer, K., Andrews, A. E., Huntzinger, D. H., ... Wei, Y. (2018). Forests dominate the interannual variability of the north american carbon sink. *Environmental Research Letters*, *13*(8), 084015. Retrieved from `http://stacks.iop.org/1748-9326/13/i=8/a=084015` doi: 10.1088/1748-9326/aad505

Smith, T. E. L., Wooster, M. J., Tattaris, M., & Griffith, D. W. T. (2011). Absolute accuracy and sensitivity analysis of op-ftir retrievals of co_2, ch_4 and co over concentrations representative of "clean air" and "polluted plumes". *Atmos. Meas. Tech.*, *4*(1), 97–116. Retrieved from https://www.atmos-meas-tech.net/4/97/2011/ doi: 10.5194/amt-4-97-2011

Tapley, B. D., Bettadpur, S., Ries, J. C., Thompson, P. F., & Watkins, M. M. (2004). Grace measurements of mass variability in the earth system. *Science*, *305*(5683), 503–505.

Tramontana, G., Jung, M., Schwalm, C. R., Ichii, K., Camps-Valls, G., Ráduly, B., ... Papale, D. (2016). Predicting carbon dioxide and energy fluxes across global FLUXNET sites with regression algorithms. *Biogeosciences*, *13*(14), 4291–4313. Retrieved from https://www.biogeosciences.net/13/4291/2016/ doi: 10.5194/bg-13-4291-2016

Vose, R., Easterling, D., Kunkel, K., LeGrande, A., & Wehner, M. (2017). Temperature changes in the united states [Book Section]. In D. Wuebbles, D. Fahey, K. Hibbard, D. Dokken, B. Stewart, & T. Maycock (Eds.), *Climate science special report: Fourth national climate assessment, volume i* (pp. 185–206). Washington, DC, USA: U.S. Global Change Research Program. doi: 10.7930/J0N29V45

Wei, Y., Liu, S., Huntzinger, D. N., Michalak, A. M., Viovy, N., Post, W. M., ... others (2014). The North American carbon program multi-scale synthesis and terrestrial model intercomparison project–Part 2: environmental driver data. *Geosci. Model Dev.*, *7*(6), 2875–2893. doi: 10.5194/gmd-7-2875-2014

Wolf, S., Keenan, T. F., Fisher, J. B., Baldocchi, D. D., Desai, A. R., Richardson, A. D., ... others (2016). Warm spring reduced carbon cycle impact of the 2012 us summer drought. *Proceedings of the National Academy of Sciences*, *113*(21), 5880–5885.

Zhang, X., Gurney, K. R., Peylin, P., Chevallier, F., Law, R. M., Patra, P. K., ... Krol, M. (2013). On the variation of regional co_2 exchange over temperate and boreal north america. *Global Biogeochemical Cycles*, *27*(4), 991–1000.